Optical design of MOIRCS

Ryuji Suzuki[a,b], Chihiro Tokoku[a,b], Takashi Ichikawa[a] and Tetsuo Nishimura[b]

[a]Astronomical Institute, Tohoku University, Sendai, Miyagi 980-8578, Japan
[b]Subaru Telescope, National Astronomical Observatory of Japan,
650 North A'ohoku Place, Hilo, Hawaii 96720, USA

ABSTRACT

We describe an optical design process and image performance evaluations for Multi-Object near-InfraRed Camera and Spectrograph (MOIRCS). MOIRCS is a near-infrared imager and multi-object spectrograph under construction for the Subaru Telescope. MOIRCS provides direct imaging of 4'×7' F.O.V. with a pixel scale of 0.12". MOIRCS also provide low-resolution multi-object spectroscopy with grisms and cooled multi-slit masks on the Cassegrain focal plane. CaF_2, BaF_2, ZnSe, and Fused Silica are used as the lens materials. They have high transmission in the near-infrared wavelength. During the design process, we find that a triplet with an achromatic doublet and a ZnSe singlet shows good performance for chromatic aberration. Therefore, we design our optics on the basis of the triplet with ZnSe. The designed optics shows good performances. Ensquared energy within 2 pixel square is more than 85 % over the entire wavelength range and F.O.V. We do not need refocusing with the change of observed wavelengths because chromatic aberration is as small as 100 μm by the triplet with ZnSe over the entire wavelength range from 0.85 to 2.5 μm. Lateral chromatic aberration of 15 μm is less than 1 pixel size. Detailed tolerance analysis is done with possible manufacturing and aligning errors considered. The result shows that designed performances will be kept with a probability of 80 % with reasonable tolerances. Ghost analysis is also done over entire F.O.V. and we find a ghost image of 13 magnitude fainter than original image that is not significant for our purpose. Therefore, we conclude that we can obtain enough performances with designed optics.

Keywords: near-infrared, multi-object spectroscopy, camera, optics, design, Subaru Telescope

1. INTRODUCTION

MOIRCS is one of the second generation instruments for the Subaru Telescope. MOIRCS has a wide field imaging mode and a multi-object spectroscopy mode. We can cover 4'×7' F.O.V. with a pixel scale of 0.12" in the imaging mode. We can also obtain many spectra at a time in the multi-object spectroscopy mode with grism and cooled multi-slit masks on the Cassegrain focal plane. The wavelength coverage is from 0.85 to 2.5 μm. Other information and discussions about MOIRCS are prepared elsewhere.[1]

When we design the optics of a wide field camera in the near-infrared wavelength with a large telescope, some difficulties always arise. First, The chromatic aberration is difficult to be corrected. This is because there are not too many materials available in the near-infrared wavelength. Secondly, the lens size becomes large because of the wide F.O.V. of the camera and a small plate scale of the large telescope. This causes difficulties in manufacturing and further reduces the number of available lens materials. Thirdly, the optics has to be cooled to cryogenic temperature, therefore we have to consider the contraction of the materials including lens mounting structures and variation of refractive index of the lens materials. The Forth is the mechanical accuracy needed. The pixel size is as small as 18 μm, and we have to keep the image quality of this size with the large optics in cryogenic temperature. We put a focus of this paper on overcoming these difficulties and designing the optics which can utilize the excellent image performance of the Subaru Telescope.

We use a commercially available optical design software, ZEMAX[2] to optimize the optics. First, we examine a doublet study then a triplet study to search for the best material combination in the selected materials. We

Further author information: (Send correspondence to RS)
RS: E-mail: ryuji@subaru.naoj.org

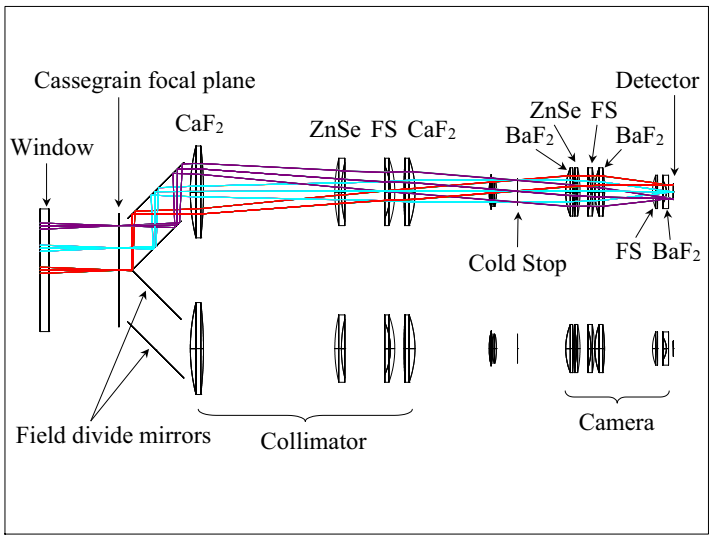

Figure 1. Layout of the optics. Rays are drawn in only one channel.

find that a triplet with an achromatic doublet and a ZnSe singlet shows a good performance. Therefore, we design the optics by using the triplet with ZnSe. The designed optics shows good performances. In the imaging mode, the ensquared energy is more than 85 % within 2 pixel square over the entire F.O.V. and the axial chromatic aberration is 100 μm over the wavelength range. In the spectroscopy mode, a good performance is obtained, however, the image quality is degraded at higher spectral resolution. The detailed tolerance analysis shows that these image qualities will be kept with a probability of 80 % when we manufacture and align the optics with the reasonable tolerances. Therefore, we conclude that we can design the optics which meets our specifications.

In the following section, we briefly review the optical system and specifications on the optics. Then we present the optical design procedure, its performances and results of some analyses. In the final section we present the precision mounting mechanism for our large lenses.

2. OPTICS OVERVIEW

First of all, we briefly describe the overview of the designed optics. Fig.1 shows an overall layout of the designed optics. We adopt a traditional collimator-camera type optics. The collimator changes light from the telescope to a parallel beam in which filters and grisms can be inserted. It also makes a sharp image of the telescope secondary mirror so that a cold stop can be placed at the pupil image position. The camera reimages the parallel beam onto the detectors. As the two HAWAII-2 detectors which we use to cover 4'×7' F.O.V. (4'×3.5' for each detector) are not buttable, we need a field divide mechanism and two sets of identical optics. Among possible field divide mechanisms, we adopt field divide mirrors which consist of a roof mirror and two fold mirrors.

Although the nominal F.O.V. of MOIRCS is 4'×7', it varies with wavelengths and observing modes. The full 4'×7' F.O.V. is available in the imaging mode at wavelength shorter than 2.1 μm, but it is limited within 6' diameter to reduce the extraneous radiation in the imaging mode at longer wavelength and in the spectroscopy mode. Fig.4 shows a configuration of the F.O.V. Although there is 1'×4' blank field (30"×4' field for each detector) in the imaging mode, it is filled by spectra in the spectroscopy mode.

3. SPECIFICATIONS

We summarize the optics specifications in Table 1. The pixel scale is determined so that we can sample adequately the best possible seeing in K-band. As a result, F.O.V. of MOIRCS in the imaging mode becomes

4'× 7' at wavelength shorter than 2.1 μm and 22 arcmin^2 at longer wavelength because of the limited F.O.V. within the 6' diameter.

The pupil size is determined after some trades. A small pupil is generally preferred because of a low cost of filters, grisms, and turrets, and also a smaller pupil makes the overall instrument length shorter because it means a shorter focal length of the collimator which has a large contribution to the overall length. The overall length of the instrument is rather critical because it is strictly constrained by the telescope interface condition. On the other hand, the smaller a pupil size is, the more difficult to obtain a high spectral resolution in the spectroscopy mode. A 50 mm diameter with the collimator focal length of 620 mm is a good compromise with which we can obtain the spectral resolution of 2000 and overall length of 1500 mm in the final design.

We place general requirements on the image quality except for excluding need of refocusing over the wavelength range. As described in the following section, correcting the axial chromatic aberration in the near-infrared wavelength is generally difficult and it makes the design challenging.

Table 1. Summary of optics specifications.

Wavelength range	0.85 μm$\sim$2.5 μm
Pixel scale	0.12"/pix
F number (camera)	3.926
Pixel size	18 μm
Pupil size	50 mm diameter
Image quality	$\geq$ 80% energy in 2 pixel square
Axial chromatic aberration	no need of refocusing
Lateral chromatic aberration	$\leq$1 pixel
Overall length	$\leq$1500 mm
Operation temperature	77 K

4. OPTICAL DESIGN

4.1. Material Selection

Before we go into the details of the design, we should discuss the available lens materials. In a refractive optics with a wide wavelength range as ours, the chromatic aberrations has been a problem. This is because there are not too many available lens materials in the near-infrared region. Oliva and Gennari[34] discussed this problem and found that BaF_2 and infrared glasses are the best combination to minimize the chromatic aberration. However, because the most of the infrared glasses have transmission decreasing in K-band in which we have the highest priority of our science, we give up to use them and search for the available lens materials. After the literature search, we choose BaF_2, CaF_2, ZnSe and Fused Silica as available materials. They have high transmission in the near-infrared wavelength and are easy for fabrication. Refractive index data at 77 K for BaF_2, CaF_2, and ZnSe are derived by using a temperature-dependent Sellmeier dispersion model (Tropf (1995)[5]). The data for Fused Silica are obtained from the Malitson (1965)[6] and in private communication and fitted by the same way as Tropf (1995) did. Our data for Fused Silica match to those of the other papers[78] within $\pm$0.0003. The thermal expansion data for the lens materials are obtained in private communication. They have been successfully used by other near-infrared instruments.

4.2. Window

A window material generally requires durability against atmospheric pressure, high transmission to longer wavelength, homogeneity and surface accuracy. In addition, available size is a key factor because the window

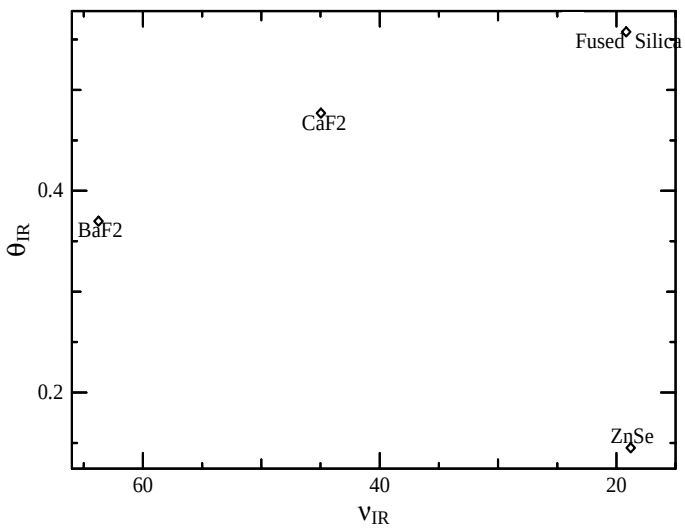

Figure 2. θ-ν diagram of the selected materials with λ_1=0.85 μm, λ_2=2.5 μm and λ_3=1.6 μm. A slope of two materials corresponds to a secondary spectrum of a doublet with the materials, as indicated by equation (1).

size becomes as large as 280 mm diameter. Under these requirements, we choose CaF_2 as the window material. The thickness (t) needed to withstand the atmospheric pressure with a safety factor of 4 is calculated by the following equation,

$$t = 1.06D\sqrt{\frac{P}{Fa}}$$

where D is a diameter of the pressured area, P is atmospheric pressure and Fa is an elastic limit of the material. We obtain the thickness of 20 mm for the CaF_2 window with additional safety factor.

4.3. Field Divide Mirrors

As mentioned in section 1, we place the field divide mirrors just below the Cassegrain focal plane to obtain wide field of view. The field divide mirrors consist of a roof mirror and two fold mirrors. The roof mirror bends the rays from the telescope 90 degree and the fold mirrors change the direction of the rays back to the same direction as the telescope optical axis, as shown in Fig.1. The roof mirror and fold mirrors are made of ULE and the surfaces are coated by gold.

4.4. Doublet and Triplet Study

To see what combination is the best in the selected materials, we calculate the axial chromatic aberration for a doublet. The secondary spectrum L of a thin, contacted doublet is written as

$$L = -\frac{\theta^{(1)} - \theta^{(2)}}{\nu^{(1)} - \nu^{(2)}} f \tag{1}$$

where

$$\nu^{(i)} = \frac{N^{(i)}(\lambda_1) - 1}{N^{(i)}(\lambda_2) - N^{(i)}(\lambda_1)}$$

$$\theta^{(i)} = \frac{N^{(i)}(\lambda_3) - N^{(i)}(\lambda_2)}{N^{(i)}(\lambda_2) - N^{(i)}(\lambda_1)}$$

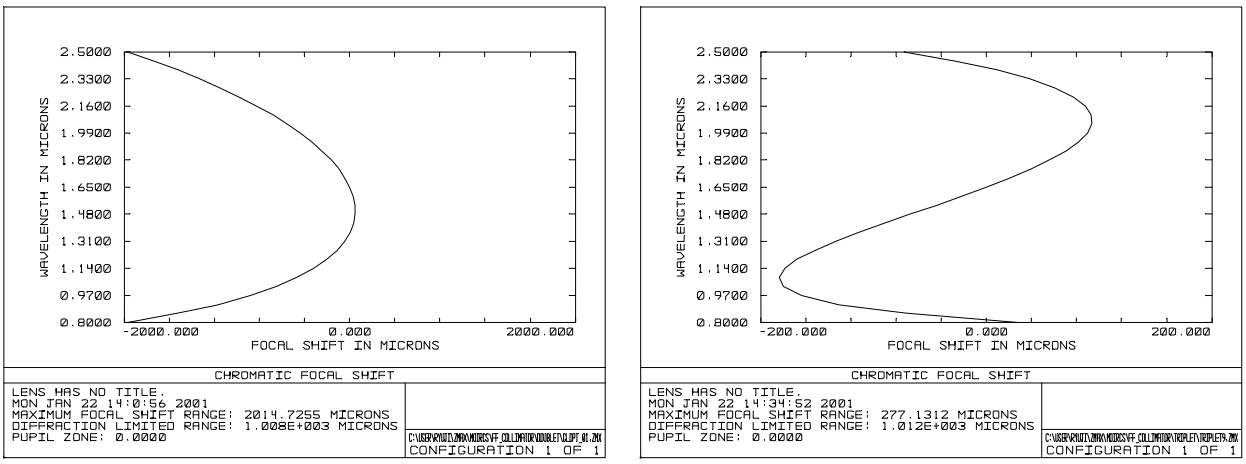

Figure 3. The axial chromatic aberration of a CaF_2-Fused Silica doublet (left) and a CaF_2-Fused Silica-ZnSe triplet (right) with a focal length of f=620 mm. The axial chromatic aberration on the detector is de-magnified to one tenth of the value indicated in the figure.

$N^{(i)}(\lambda)$, $\nu^{(i)}$, and $\theta^{(i)}$ is a refractive index at the wavelength λ, the Abbe number, and the relative partial dispersion of the ith lens material respectively. f is a focal length of the doublet. λ_1 and λ_2 are the two wavelengths at which the secondary spectrum is zero. Fig.2 shows a θ-ν diagram for the selected materials with λ_1=0.85 μm, λ_2=2.5 μm and λ_3=1.6 μm. It indicates the goodness of the material combination by its slope: the shallower the slope, the better the combination as indicated by the equation (1). We can not see any good combinations in the selected materials. Fig.3 (left) shows an example of the axial chromatic aberration of CaF_2-Fused Silica doublet whose focal length is the same as that of the collimator. We can see a large secondary spectrum of 2 mm. Though it is actually scaled down to 0.2 mm on the detector by the magnification between the camera and the collimator but is not acceptable with our specification. Because of the lack of the good material combination, we, next, examine a triplet on the basis of the doublet results. During searching the best third material, we find that adding a ZnSe lens of slightly negative power to the doublet provides a good performance, showing axial chromatic aberration of 0.3 mm (which is 0.03 mm on the detector) in the best case. Fig.3 (right) shows an example of the axial chromatic aberration of CaF_2-Fused Silica-ZnSe triplet. This ZnSe effect can be seen in any combinations with the doublet that shows a positive secondary spectrum as shown in Fig.3 (left), if ZnSe is placed where a marginal ray height is high. On the basis of the triplet result, we design the optics configuration by using the triplets with ZnSe.

4.5. Design Procedures

We use ZEMAX during the design process. ZEMAX is a very useful software especially with its global optimization and multi-configuration design features. Tolerance analysis and ghost analysis are also done by ZEMAX.

We perform the optical design in the following procedure. We design the collimator prior to the camera. First, the collimator is designed in a reverse direction; parallel rays are entered from the direction of the cold stop to the Cassegrain focal plane. At this time, the collimator should make an image on the Cassegrain focal plane, as well as its exit pupil image on the telescope secondary mirror position. After obtaining some solutions, we place it in a proper position behind the telescope. Because the collimator should make a collimated beam and a sharp image of the telescope secondary mirror, we use a multi-configuration feature to optimize both functions simultaneously. We evaluate the quality of the collimated beam by using a paraxial lens at the cold stop position. Then the camera is designed to compensate aberrations of the collimator and make a sharp image onto the detector.

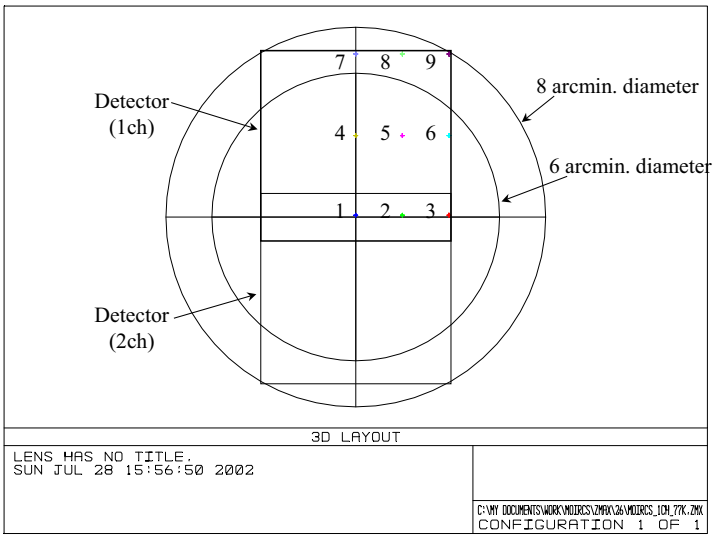

Figure 4. Configuration of the F.O.V. of MOIRCS. Nine test points used in the performance analysis are defined. Two squares show scaled detector size at the Cassegrain focal plane (thick and thin square represents the first and second channel of the two detectors respectively) and two circles show 8' and 6' diameters. A side of the square corresponds to 4'. Overlapping 1'×4' between two detectors results in 4'×7' F.O.V. in the imaging mode at wavelength shorter than 2.1 μm. F.O.V. is limited within 6' diameter in the imaging mode at longer wavelength and in the spectroscopy mode.

4.6. Collimator

The outline of the collimator design is as follows: The axial chromatic aberration and spherical aberration should be compensated by a triplet in the area where the marginal ray height is high. Although a field lens is needed, the axial chromatic aberration and the spherical aberration is negligible due to the low marginal ray height and by using a low dispersion material. The lateral chromatic aberration and coma aberration do not need to be corrected because they are compensated by the camera. On the basis of this outline, we adopt CaF_2-Fused Silica-ZnSe triplet and CaF_2 singlet as a field lens as shown in Fig.1. An air-spaced triplet is the result of correcting aberration and avoiding ghost images.

4.7. Camera

The outline of the camera design is almost the same as the collimator except we have to consider all the aberrations. As a result, we adopt BaF_2-ZnSe-Fused Silica-BaF_2 quartet and Fused Silica-BaF_2 doublet as a field flattener as shown in Fig.1. Because there is no realistic solution with BaF_2-Fused Silica doublet showing achromatic feature of equation (1) owing to a short focal length and a small difference between the two Abbe number, we split BaF_2 into two lenses and that creates a quartet instead of a triplet. The axial chromatic aberration and spherical aberration are corrected by the quartet. The lateral chromatic aberration can be adjusted by changing the combination of the materials of the field flattening doublet. The astigmatism and coma can be adjusted by bending the quartet and by changing the space between quartet and doublet.

5. PERFORMANCE

5.1. Imaging Mode

In this section, we evaluate the performances of the designed optics. First, we have to specify the evaluated field positions. Fig.4 shows the defined field positions from 1 to 9. We sample the field positions equally over the F.O.V., because our optics is not entirely axial symmetric.

Fig.5 and Fig.6 shows some results of the performance analyses in the imaging mode. Fig.5 (left) shows a spot diagram, where the field positions defined in Fig.4 are indicated from 1 (top) to 9 (bottom) along the

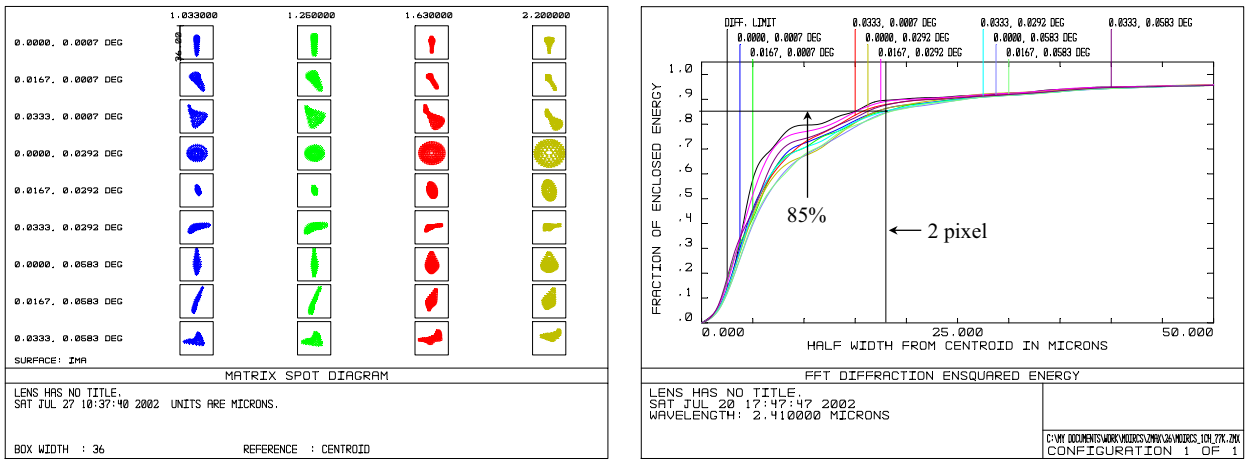

Figure 5. Spot diagram of the imaging mode (left): Vertical arrangement indicates nine field positions defined in Fig.4 from 1 (top) to 9 (bottom), while horizontal arrangement indicates central wavelengths of z, J, H, K-band from left to right. The box is the area of 2 pixel square.
Diffraction ensquared energy distribution at 2.5 μm (right): Nine field positions are shown with different lines. A vertical solid line represents 2 pixel size, while a horizontal line represents 85 % of the entering energy.

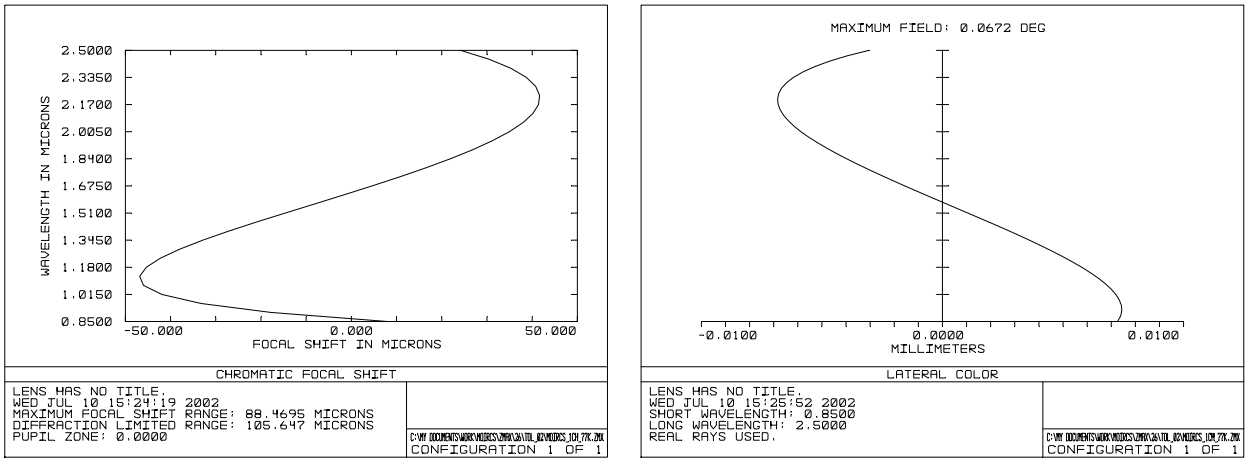

Figure 6. Axial chromatic aberration (left) and lateral chromatic aberration (right).

vertical axis and the central wavelengths from z-band (left) to K-band (right) are indicated along the horizontal axis. Superimposed square corresponds to 2 pixel square. We can see that a light from a point source is imaged within 1 or 2 pixel square for the entire F.O.V. and the wavelength range. Fig.5 (right) shows the result of a diffraction based image analysis in K-band. The energy within 2 pixel square exceeds 85 % for the entire F.O.V. Fig.6 shows the axial chromatic aberration and the lateral chromatic aberration. The axial chromatic aberration of 0.1 mm is good enough so that we do not need refocusing of the camera for different wavelengths. The lateral chromatic aberration is smaller than 1 pixel for the entire wavelength range. Therefore, there is no difference of image positions for different wavelengths.

5.2. Spectroscopy Mode

Fig.7 shows spot diagrams of the spectroscopy mode in the wavelength range from 2.0 μm to 2.5 μm with a spectral resolution of 500 and 1000. The slit width is assumed to be 0.5". We can see that most of the images

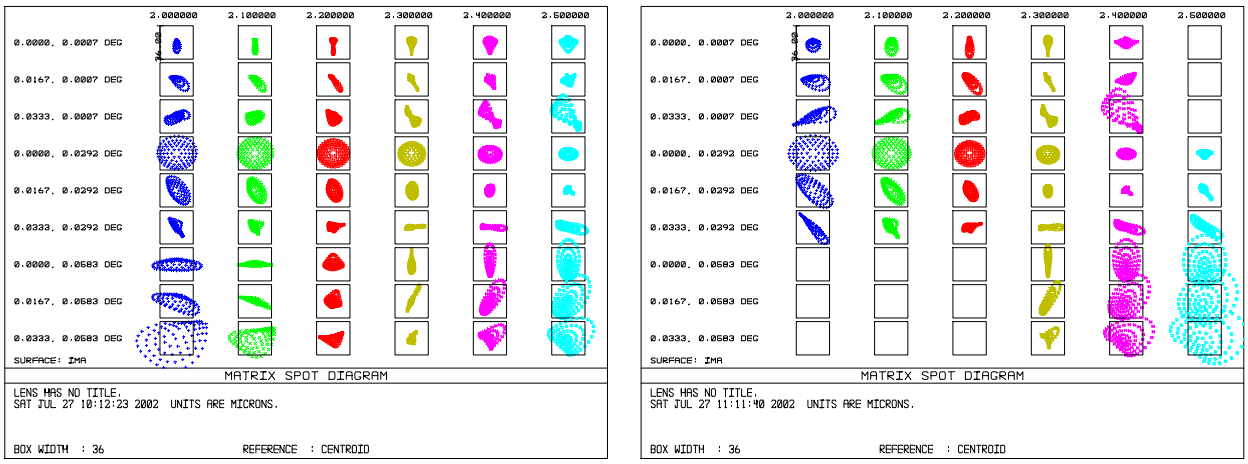

Figure 7. Spot diagram of the spectroscopy mode in the wavelength range from 2.0 μm to 2.5 μm. Spectral resolution of 500 (left) and 1000 (right) are shown. The vertical arrangement is the same as Fig.5, while the horizontal arrangement ranges from 2.0 μm to 2.5 μm. Spots that are not shown mean that they are out of the detector coverage. The box represents 2 pixel square.

are within 2 pixel squares, but they are worse than those of the imaging mode. We can also see that images get worse with higher spectral resolution. This image degradation is caused by a field curvature of the collimator which is almost determined by its focal length. At a higher spectral resolution mode, therefore, a spectral range is limited by this image degradation.

5.3. Pupil image

Finally we check how well the collimator images the telescope secondary mirror onto the cold stop. Fig.8 shows a spot diagram of the peripheral points of the telescope secondary mirror for the entire wavelength range. Ray-tracing was done with a square aperture at the Cassegrain focal plane. Because blocking the extraneous radiation is important at the longer wavelengths, we put the highest priority on the wavelengths longer than 2 μm during the optimization process. We estimate that extraneous radiation added by this image quality is less than 3 % of the radiation from the sky.

6. ANALYSIS

We perform a detailed tolerance analysis in order to estimate the actual performance of the designed optics when we manufacture and align it. For a realistic estimate, we consider manufacturing information from a lens vendor, detailed mechanism of the lens mounting and related manufacturing errors, and alignment procedure. The analysis is done by using a tolerance analysis task of ZEMAX. It creates one hundred of random optics with the specified tolerance items by a Monte-Carlo algorithm and we evaluate the performance of all these optics created. Because we plan to equip a focus adjustment mechanism, the distance between the last surface of the lens and the detector surface is used as a compensator.

The tolerance items considered are the radius of the lens surface (TRAD), center thickness of the lens and airspace between the lenses (TTHI), decenter of the lens (TED), tilt of the lens (TET), surface irregularity (TEXI), and index of refraction (TIND). TRAD, TTHI, and TEXI are the accuracies of measurements and are provided by the lens vendor. TED and TET are determined by considering a lens mounting mechanism, information from the lens vendor, surface irregularity of the optical bench, and alignment accuracy. TIND is assumed to be ± 0.0005 for all the materials.

The final evaluation is done with the diffraction based image analysis after some quick evaluations with the spot diagram. Fig.9 shows the result of the tolerance analysis. We can see that the good image performance,

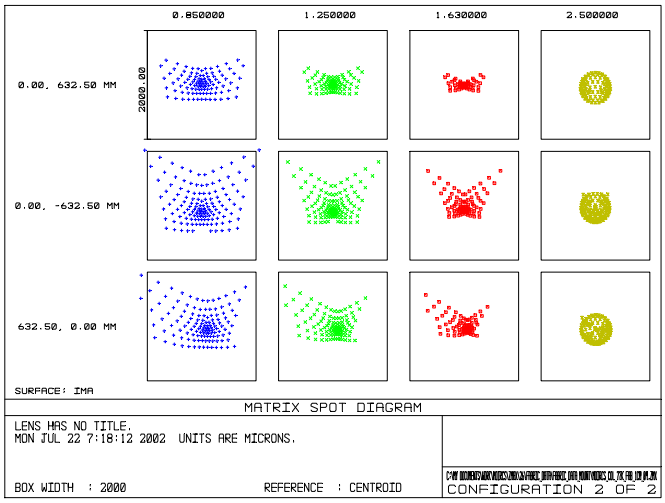

Figure 8. Spot diagram of the telescope secondary mirror. The coordinates of the peripheral points on the telescope secondary mirror (top, bottom and right side) are indicated vertically, while wavelengths in μm are indicated horizontally. The box represents 2 mm square, while the cold stop size is 50 mm diameter.

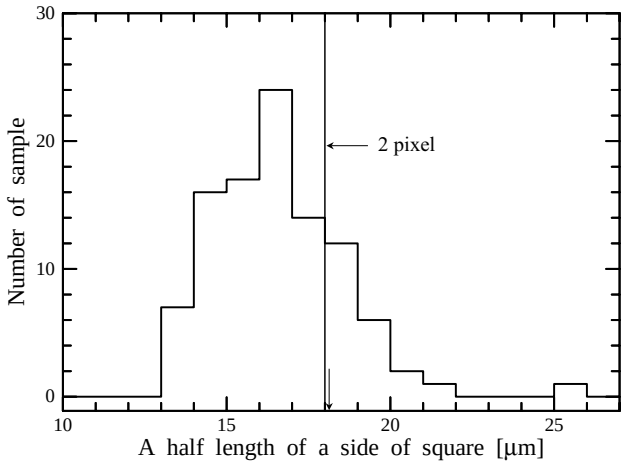

Figure 9. Result of the tolerance analysis. Horizontal axis indicates a half of a side length of square in which 80 % of the entering energy are enclosed for the entire F.O.V. Vertical axis indicates the number of sample optics within each bin. A superimposed arrow means a position of the 80th sample from the best case among 100 samples totally produced by the Monte-Carlo simulation. The vertical solid line represents a 2 pixel.

which is defined as whether or not 80 % of the entering energy are enclosed within 2 pixel square, is kept with a probability of 80 % when we manufacture and align the optical components with reasonable tolerances. A similar Monte-Carlo tolerance analysis for only the collimator shows no significant degradation of the pupil image and parallelism of the collimated beam.

We also perform a ghost analysis by using "Ghost Focus Generator" in ZEMAX. This task changes all the refractive surfaces to the reflective surfaces and ray-tracing is done. We assume reflectivity of 2 % per lens surface, 40 % for the detector surface, 10 % for the filter surface and 100 % for the back side of the slit mask.

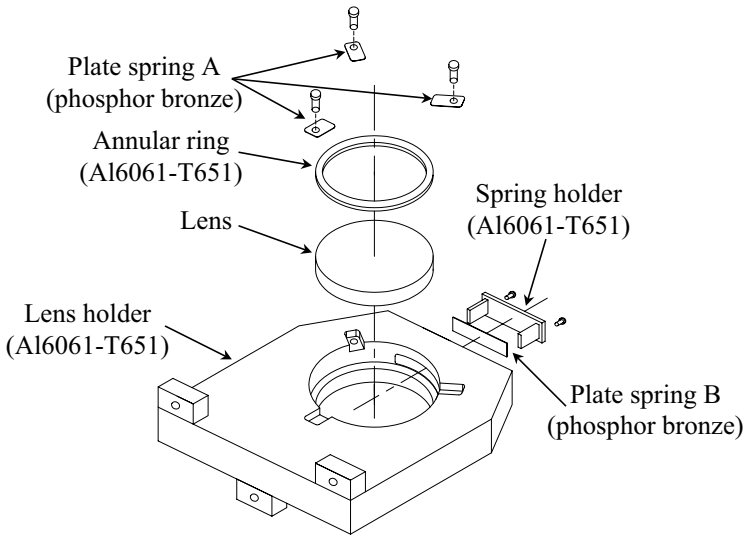

Figure 10. Layout of the mounting mechanism of the lens. Plate spring A and B push the lens to each direction against the contact surface of the mount. Plate spring A are screwed on the mount, while plate spring B is pushed by spring holder which is screwed on the mount. The mount is fixed on the optical bench by three tabs shown in bottom left.

The analysis is done for the entire F.O.V. and the result shows that a ghost image of 13 magnitude fainter than original image is generated near the center of the F.O.V. However, this result is satisfactory for our purpose.

7. MOUNTING METHOD

In this section, we briefly describe a mounting method of our lenses. To keep the designed performances, we need a precision mounting method of the lens at 77 K. For the precision mounting at cryogenic temperature, a thermal treatment and predictability of the thermal contraction of the material of the mount are important as well as the machining accuracy. We adopt Al6061-T651 with a further heat treatment (uphill quenching) because Al6061-T651 has already undergone a normal heat treatment and the amount of thermal contraction at 77 K is known. The uphill quenching is needed to release the residual stress generated by the machining and prevent deformation at 77 K. The process consists of a thermal cycle between 77 K, 283K, and room temperature. We carry out the thermal cycles five times after a rough machining, and then the final machining is done. Fig.10 shows a layout of our mounting mechanism. Four plate springs made of phosphor bronze are used to hold the lens and release extra stress caused by the thermal contraction difference between Al6061-T651 and the lens material. Three plate springs (spring A) push the lens to axial direction by way of an annular ring, and one plate spring (spring B) pushes the lens to the direction perpendicular to the optical axis. We estimate the induced stress by the plate springs at 77 K both analytically and by simulation with Finite Element Method and confirm that there is no such stresses as to break the lens for all the lens mounts.

8. CONCLUSION

The designed optics shows good performances both in the imaging mode and the spectroscopy mode. The collimator provides the collimated beam and the good image of the telescope secondary mirror. The ghost image is generated, but is not significant for our purpose. We can obtain the designed performance with a probability of 80 % with realistic tolerances. Therefore, we conclude that we can obtain good image quality with the designed optics.

9. ACKNOWLEDGMENTS

We would like to thank Naoto Kobayashi of the Subaru Telescope for a discussion and providing us a lot of literatures on near-infrared optics. We would also like to thank Kunio Takeshi of Canon Inc. and Roland Sarlot of the Stewart Observatory for reviewing our optics and giving helpful comments.

This research was supported by grant-in-aid from scientific research of the Ministry of Education, Culture, Sports, Science and Technology (09440088, 11554005).

REFERENCES

1. C. Tokoku, T. Ichikawa, R. Suzuki, K. Asai, Y. Katsuno, K. Omata, T. Yamada, T. Tsuda, T. Chiba, A. Sasaki, and T. Nishimura , "MOIRCS: Multi-Object Infrared Camera and Spectrograph for the Subaru Telescope," in *Instrument Design and Performance for Optical/Infrared Ground-based Telescopes*, M. Iye and F. Moorwood, eds., *Proc. SPIE* **4841**, 2002.
2. Focus Software Inc., P.O. Box 18228, Tucson, AZ, 85731.
3. E. Oliva and S. Gennari, "Achromatic lens systems for near infrared instruments," *Astron. Astrophys. Suppl. Ser. 114* , pp. 179–182, 1995.
4. E. Oliva and S. Gennari, "Achromatic lens systems for near infrared instruments II. Performances and limitations of standard Flint glasses," *Astron. Astrophys. Suppl. Ser. 128* , pp. 599–603, 1998.
5. W. J. Tropf, "Temperature-dependent refractive index models for BaF_2, CaF_2, MgF_2, SrF_2, LiF, NaF, KCl, ZnS and ZnSe," *Optical Engineering* **34**, pp. 1369–1373, 1995.
6. I. H. Malitson, "Interspecimen Comparison of the Refractive Index of Fused Silica," *J. Opt. Soc. Am.* **55**, pp. 1205–1209, 1965.
7. J. Matsuoka, N. Kitamura, S. Fujinaga, T. Kitaoka and H. Yamashita, "Temperature dependence of refractive index of SiO_2 glass," *J. Non-Cry. Sol.* **135**, pp. 86–89, 1991.
8. J. H. Wray and J. T. Neu, "Refractive Index of Several Glasses as a Function of Wavelength and Temperature," *J. Opt. Soc. Am.* **59**, pp. 774–776, 1969.